

Extraction of accurate structure-factor amplitudes from Laue data: wavelength normalization with wiggler and undulator X-ray sources

Vukica Šrajer,^{a,b*} Sean Crosson,^a Marius Schmidt,^a Jason Key,^a Friedrich Schotte,^c Spencer Anderson,^a Benjamin Perman,^a Zhong Ren,^{a,b} T. Y. Teng,^{a,b} Dominique Bourgeois,^{c,d} Michael Wulff^c and Keith Moffat^{a,b}

^aDepartment of Biochemistry and Molecular Biology, The University of Chicago, 920 East 58th Street, Chicago, IL 60637, USA, ^bConsortium for Advanced Radiation Sources, The University of Chicago, 5640 South Ellis Avenue, Chicago, IL 60637, USA, ^cEuropean Synchrotron Radiation Facility, BP 220, 38043 Grenoble CEDEX, France, and ^dUPR 9015/IBS, 41 Avenue des Martyrs, 38027 Grenoble, France. E-mail: vusr@midway.uchicago.edu

(Received 24 January 2000; accepted 23 March 2000)

Wavelength normalization is an essential part of processing of Laue X-ray diffraction data and is critically important for deriving accurate structure-factor amplitudes. The results of wavelength normalization for Laue data obtained in nanosecond time-resolved experiments at the ID09 beamline at the European Synchrotron Radiation Facility, Grenoble, France, are presented. Several wiggler and undulator insertion devices with complex spectra were used. The results show that even in the most challenging cases, such as wiggler/undulator tandems or single-line undulators, accurate wavelength normalization does not require unusually redundant Laue data and can be accomplished using typical Laue data sets. Single-line undulator spectra derived from Laue data compare well with the measured incident X-ray spectra. Successful wavelength normalization of the undulator data was also confirmed by the observed signal in nanosecond time-resolved experiments. Single-line undulators, which are attractive for time-resolved experiments due to their high peak intensity and low polychromatic background, are compared with wigglers, based on data obtained on the same crystal.

Keywords: Laue X-ray diffraction; wavelength normalization; insertion devices.

1. Introduction

1.1. Laue experiments and choice of insertion device

The Laue X-ray diffraction technique facilitates rapid data collection by taking advantage of polychromatic X-ray sources. The exposure times are reduced by three to four orders of magnitude as compared with the conventional monochromatic diffraction technique (Moffat, 1997). Exposure times as short as 150 ps are sufficient when using high-brilliance X-ray sources such as insertion devices at third-generation synchrotron sources (Szebenyi *et al.*, 1992; Bourgeois *et al.*, 1996). The exciting prospect of investigating fast structural changes in biological macromolecules materialized in the first nanosecond time-resolved Laue X-ray diffraction studies of photosensitive proteins (Šrajer *et al.*, 1996; Perman *et al.*, 1998).

In order to conduct successful Laue experiments it is important to consider spectral properties of the X-ray radiation delivered to the sample. The minimum and maximum wavelengths at which significant intensity is present are denoted λ_{\min} and λ_{\max} , respectively. They define the spectral bandpass of the source, $\lambda_{\max} - \lambda_{\min}$.

Advances in Laue data processing during the last decade (Campbell & Hao, 1993; Ren & Moffat, 1995a,b; Bour-enkov *et al.*, 1996; Bourgeois *et al.*, 1998; Clifton *et al.*, 1997) addressed and resolved the energy and spatial overlap problems, traditionally considered problems serious enough to limit the use of the technique. This significantly improved the quality and completeness of Laue data collected using more standard broad-bandpass sources such as bending magnets and wigglers, and led to a wider use of the Laue technique (Ren & Moffat, 1995a,b; Šrajer *et al.*, 1996; Perman *et al.*, 1998; Yang *et al.*, 1998; Ravelli *et al.*, 1999; Nieh *et al.*, 1999; Ren *et al.*, 1999). Sources with a relatively narrow spectral bandpass, such as single-line undulators, reduce harmonic and spatial overlaps as well as the polychromatic background in typically crowded Laue patterns (Moffat *et al.*, 1984; Bartunik & Borchert, 1989; Bartunik *et al.*, 1992; Moffat, 1997; Ren *et al.*, 1999). An improved signal-to-noise ratio is expected to result from their use.

The results we present here address the choice of the X-ray source for Laue experiments. Can we derive satisfactory structure-factor amplitudes when the X-ray spec-

trum is complex, with sharply varying features as in the case of wigglers and undulators? Can we derive satisfactory structure-factor amplitudes from the data collected using single-line undulators where the intensity variations with wavelength are extreme and the spectral bandpass is very narrow? Are single-line undulators better for Laue experiments than wigglers due to a reduced background and, consequently, enhanced signal-to-noise ratio?

1.2. Wavelength normalization in Laue data processing

In a Laue diffraction experiment each measurement of the intensity of a Laue spot must be corrected by a number of factors to enable the structure-factor amplitude to be obtained (Ren & Moffat, 1995*a*). One such factor contains all wavelength-dependent effects and is known as the wavelength-normalization curve or λ -curve. This factor includes variation of the incident X-ray intensity with wavelength, diffraction efficiency, the overall absorption correction including the absorption by the crystal and the mount, and the wavelength-dependent response of the detector.

The most accurate and most reliable method for wavelength normalization uses Laue data. Intensities of symmetry-related reflections stimulated by different wavelengths are compared to derive the λ -curve (Campbell *et al.*, 1986; Helliwell *et al.*, 1989; Ren & Moffat, 1995*a,b*). Chebyshev polynomials are used to model the curve accurately (Smith Temple, 1989; Ren & Moffat, 1995*a*; Arzt *et al.*, 1999).

Challenging tests for the wavelength normalization are presented by spectra with very sharp intensity variation as a function of wavelength. This is the case when the absorption edges from mirrors or detectors are present or when

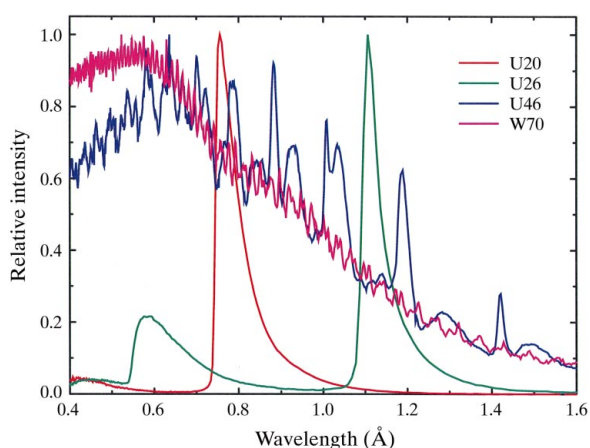


Figure 1 Measured spectra of insertion devices W70 (20.1 mm), U46 (16.4 mm), U26 (17 mm) and U20 (16.3 mm) at the ID09 beamline (ESRF, Grenoble, France). Spectra are measured by scanning the monochromator and measuring intensity through a 0.2 mm × 0.2 mm pinhole at the sample position by a PIN diode. Spectra are corrected for the wavelength response of the diode used for intensity measurements.

wigglers and undulators are used as X-ray sources. The Chebyshev polynomial method handles the problem of sharp spectral features by increasing the degree of the polynomial. A compromise is necessary to accurately account for sharp features but to avoid fitting the noise with higher-order polynomials. The method has been already used to model X-ray spectra containing absorption edges. The Pt edges (L_I , L_{II} and L_{III}) arising from the focusing mirror at beamline X26C (NSLS, Brookhaven National Laboratory) were successfully modeled by a 64-degree Chebyshev polynomial (Ren & Moffat, 1995*a*; Yang *et al.*, 1998). The method was also applied to analyze the first Laue patterns recorded with a 120 ps exposure using an undulator X-ray source (Szebenyi *et al.*, 1992). The λ -curve was derived from five images using a 300-degree Chebyshev polynomial. The curve parallels the ratio of Laue intensities (corrected for all factors except wavelength dependence) and the corresponding monochromatic intensities [see Fig. 3 of Szebenyi *et al.* (1992)].

We report further evidence of the ability of the Chebyshev polynomial method to derive sharply varying λ -curves from Laue data collected using wiggler and undulator sources. We also assess, to a limited degree, the relative merits of wiggler and undulator sources. Laue data from both sources yielded structure-factor amplitudes of accuracy comparable with those from monochromatic data, and capable of revealing small structural changes in nanosecond time-resolved experiments.

2. Experimental methods

The data were obtained during nanosecond time-resolved experiments conducted at the ID09 beamline at the European Synchrotron Radiation Source (ESRF) in Grenoble, France. The beamline accommodates up to three insertion devices that can be used independently or combined (Wulff *et al.*, 1997). The insertion devices include two wigglers (or undulators), U46 (46 mm period, 71 poles, $E_f = 1.60$ keV, $K = 2.72$) and W70 (70 mm period, 43 poles, $E_{crit} = 20$ keV, $K = 5.40$), as well as two single-line undulators, U26 (26 mm period, 129 poles, $E_f = 11.02$ keV, $K = 0.65$) and U20 (20 mm period, 162 poles, $E_f = 16.70$ keV, $K = 0.27$). This beamline is designed for time-resolved experiments in macromolecular crystallography and liquids, and high-pressure experiments (Wulff *et al.*, 1997). For time-resolved experiments the white beam is focused by a Pt-coated toroidal mirror and delivered to the experimental station with an energy range of 5–38 keV. Directly measured X-ray spectra incident at the sample for W70, U46, U26 and U20 are shown in Fig. 1.

The experimental protocol and the data-collection method are described by Bourgeois *et al.* (1996). Data were collected using carbonmonoxy myoglobin (MbCO) crystals, space group $P2_1$, and photoactive yellow protein (PYP) crystals, space group $P6_3$. The data were collected using single- and super-bunch modes of the ESRF storage ring. In

Table 1

Data-collection parameters and data-reduction statistics for W70 and U26.

	W70	U26
Crystal type	PYP	PYP
Exposure time	1 μ s	1 μ s
Number of exposures per frame	4	2
Number of frames per data set	32	60
Angular increment	2°	1°
Singles		
Observations†	85617	53943
Unique reflections	8432	3960
Overall redundancy	10.1	13.6
$R_{\text{merge}}(F^2)$ (%)‡	12.4	12.3
$R_{\text{merge}}(F)$ (%)§	4.7	5.2
Intensity		
	$R_{\text{merge}}(F)$ (%)	
28–68	26.6	16.2
68–161	17.9	11.4
161–382	11.6	7.9
382–909	7.8	5.6
909–2161	4.4	4.0
2161–5136	2.7	3.2
5136–12207	2.0	2.9
12207–29015	1.6	3.1
Resolution range (Å)		
	Completeness (%) / $R_{\text{merge}}(F)$ (%)	
100–3.60	70.0/2.8	87.8/4.4
3.60–2.86	89.9/4.6	97.6/6.1
2.86–2.50	92.4/8.0	87.4/8.6
2.50–2.27	93.7/10.3	49.7/9.9
2.27–2.10	93.3/11.8	1.8/12.1
2.10–1.98	91.2/12.7	–
1.98–1.88	85.0/13.7	–
1.88–1.80	80.8/13.5	–
Singles and multiples combined		
Unique reflections¶	9044	4081
Resolution range		
	Completeness (%)	
100–3.60	91.6	96.0
3.60–2.86	96.3	98.5
2.86–2.50	97.1	87.5
2.50–2.27	96.0	49.8
2.27–2.10	95.4	1.8
2.10–1.98	93.9	–
1.98–1.88	89.1	–
1.88–1.80	84.6	–

† Observation with $I/\sigma_I > 0.5$, where I is the intensity of the observed reflection from a profile fit and σ_I is the residual from the fit. All data were integrated to 1.8 Å resolution. ‡ $R_{\text{merge}}(F^2)$ (%) = $\sum w(|F^2| - F^2) / \sum w F^2$, where F^2 is the square of the structure-factor amplitude of an observed reflection, calculated by scaling the measured intensity by a generalized scale factor, $\langle F^2 \rangle$ is the average of F^2 from multiple observations and $w = 1/\sigma^2(F^2)$ is the weight (Ren & Moffat, 1995a). § $R_{\text{merge}}(|F|)$ (%) = $\sum w(|F|) - |F| / \sum w |F|$, where $|F|$ is the structure-factor amplitude and $\langle |F| \rangle$ is the average amplitude from multiple observations. ¶ Unique reflections with $F/\sigma_F > 2$, where σ_F is the r.m.s. deviation determined from merging of structure amplitudes.

the single-bunch mode the duration of the X-ray pulse is 150 ps. In order to improve the signal-to-noise ratio, each image was derived from 10–30 exposures to single X-ray pulses prior to detector readout. In the super-bunch mode the X-ray pulse duration is ~ 1 μ s and exposures to 1–4 pulses per frame were typical. We used the following

Table 2

Data-collection parameters and data-reduction statistics for U20.

Crystal type	MbCO
Exposure time	150 ps
Number of exposures per frame	10
Number of frames per data set	90
Angular increment	2°
Singles	
Observations†	18336
Unique reflections	7923
Overall redundancy	2.3
$R_{\text{merge}}(F^2)$ (%)‡	8.3
$R_{\text{merge}}(F)$ (%)§	3.5
Intensity	
	$R_{\text{merge}}(F)$ (%)
22–72	13.1
72–239	9.7
239–792	6.3
792–2623	3.9
2623–8682	2.4
8682–28737	2.0
28737–95119	2.3
95119–314838	2.6
Resolution range (Å)	
	Completeness (%) / $R_{\text{merge}}(F)$ (%)
100–3.60	94.6/2.9
3.60–2.86	92.7/3.4
2.86–2.50	83.9/4.6
2.50–2.27	74.7/5.1
2.27–2.10	60.1/6.2
2.10–1.98	48.8/7.4
1.98–1.88	32.7/8.1
1.88–1.80	25.0/8.9
Singles and multiples combined	
Unique reflections¶	8021
Resolution range	
	Completeness (%)
100–3.60	96.3
3.60–2.86	94.4
2.86–2.50	85.9
2.50–2.27	75.0
2.27–2.10	60.1
2.10–1.98	48.8
1.98–1.88	32.7
1.88–1.80	25.0

† Observation with $I/\sigma_I > 0.5$, where I is the intensity of the observed reflection from a profile fit and σ_I is the residual from the fit. All data were integrated to 1.8 Å resolution. ‡ $R_{\text{merge}}(F^2)$ (%) = $\sum w(|F^2| - F^2) / \sum w F^2$, where F^2 is the square of the structure-factor amplitude of an observed reflection, calculated by scaling the measured intensity by a generalized scale factor, $\langle F^2 \rangle$ is the average of F^2 from multiple observations and $w = 1/\sigma^2(F^2)$ is the weight (Ren & Moffat, 1995a). § $R_{\text{merge}}(|F|)$ (%) = $\sum w(|F|) - |F| / \sum w |F|$, where $|F|$ is the structure-factor amplitude and $\langle |F| \rangle$ is the average amplitude from multiple observations. ¶ Unique reflections with $F/\sigma_F > 2$, where σ_F is the r.m.s. deviation determined from merging of structure amplitudes.

insertion devices and their combinations: W70, W70 + U46 tandem, U26 and U20.

The number of frames needed for a complete Laue data set is determined by the angular increment $\Delta\varphi$ between the consecutive spindle angles that is necessary to cover the reciprocal space at a resolution d (Ren *et al.*, 1999),

$$\Delta\varphi = \sin^{-1}(\lambda_{\text{max}}/2d) - \sin^{-1}(\lambda_{\text{min}}/2d).$$

It is evident from the expression above that a large angular increment in crystal orientation reduces completeness

much more at low resolution than at high resolution (Moffat, 1997; Ren *et al.*, 1999). With the W70 wiggler or with the U46 + W70 tandem, a typical MbCO data set consisted of about 40–45 frames, where crystals were rotated through 180° with a 4–5° angular increment. For PYP crystals, about 30 frames were typically collected during 60° crystal rotation with a 2° angular increment. The narrow-bandpass undulators U26 and U20 required smaller angular increments. For example, an increment of 1° is needed to collect data complete at 4 Å resolution with U20. This requires at least 180 frames for Mb crystals and 60

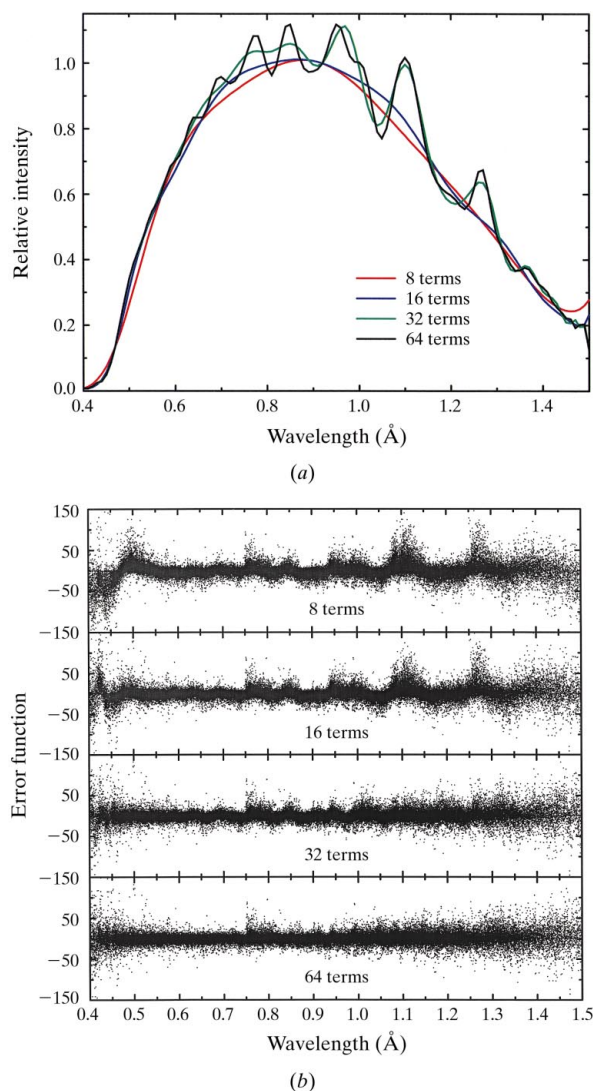


Figure 2

(a) The W70 + U46 wavelength-normalization curve modeled by an increasing number of Chebyshev terms: 8, 16, 32 and 64, to account for the U46 features in the W70 + U46 spectrum. Two myoglobin data sets are scaled together to derive the curve (145 ns photoproduct Mb* and MbCO, 49 frames each, 4° angular increment). (b) Plot of the error function $(F^2 - \langle F^2 \rangle) / \sigma_{(F^2)}$ versus wavelength (Ren & Moffat, 1995a). An increased number of Chebyshev terms improves modeling of U46 spectrum and results in reducing the residual error function ripples.

frames for PYP crystals. In order to improve redundancy and completeness of the data, we collected data with a 0.5° angular increment in some cases. The large number of frames per data set increases fourfold the total elapsed time for data-set collection. This makes a significant difference, between 1.5 and 6 h in the case of Mb data collection, for example.

Data were processed using *LaueView* software (Ren & Moffat, 1995a,b). We stress again that the λ -curve derived from the data by *LaueView* includes all wavelength-dependent effects. The crystal absorption is not treated separately and the λ -curve derived for different size crystals will differ due to the difference in absorption. Examples of typical data-collection information and data-reduction statistics for W70, U26 and U20 data are given in Tables 1 and 2.

The λ -curve was not always derived from one complete data set. In some cases it was derived by scaling together more than one data set collected under similar experimental conditions, using the same crystal. For example, an MbCO photoproduct data set (Mb*), where the crystal was illuminated by a short laser pulse prior to each X-ray pulse, and the corresponding MbCO data set collected on the same crystal, were typically scaled together. In the case of undulator data sets that consist of more than 100 frames, we used only part of the data set to derive the λ -curve. This is partly due to the fact that the derivation does not require a complete data set. In fact, a λ -curve can be determined quite reliably from only a few frames (see §3). This holds even for undulator spectra where high-degree Chebyshev polynomials have to be used and a large number of observations are needed to determine all the polynomial

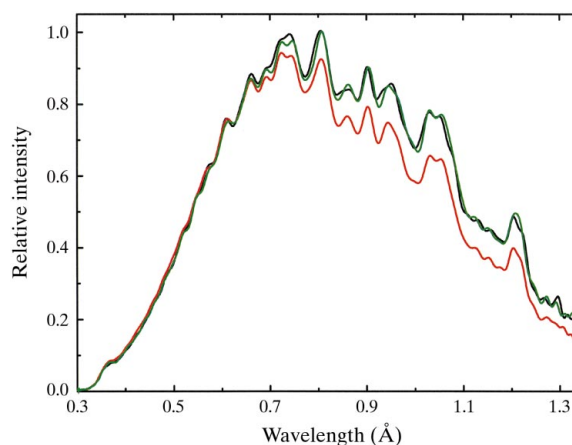


Figure 3

Reproducibility of the wavelength normalization for the W70 + U46 tandem. MbCO data from three different crystals are used. The λ -curves are modeled with 128 Chebyshev terms. Undulator ripples are reproduced in position and amplitude. Two curves, which agree well with each other (black and green), are from data collected on crystals of the same size (0.45 mm × 0.45 mm × 0.1 mm), while the third one (red) is derived from data collected using a larger crystal (0.60 mm × 0.30 mm × 0.15 mm).

coefficients. A minor technicality also prevented us from using complete undulator data sets: the present *LaueView* processing software is limited to scaling of ≤ 100 individual frames.

3. Results and discussion

3.1. Wavelength normalization for W70 + U46 data

In order to boost the X-ray flux for nanosecond time-resolved experiments, we often used two insertion devices, W70 and U46, in series. The wavelength-normalization curve for this tandem, derived from MbCO data, is shown in Fig. 2(a). The W70 + U46 curve is modeled by Chebyshev polynomials of a progressively increased degree, from eight to 64 polynomial terms. The increased number of polynomial terms clearly reveals small ripples in the spectrum. Are they real? This can be judged from the so-called ‘error’ plots (Ren & Moffat, 1995a) shown in Fig. 2(b). When the ‘error’ $(F^2 - \langle F^2 \rangle) / \sigma_{(F^2)}$ (Ren & Moffat, 1995a) is plotted against wavelength, it reveals that an increase of Chebyshev terms from eight to 64 leads to an increasingly smoother and more horizontal plot. Any residual systematic deviation from the horizontal line centered at zero indicates that wavelength normalization is not completed. As the number of Chebyshev terms is increased further, artifactual small-amplitude ripples will appear in the truly smooth parts of the spectrum while continuing to improve the fit to features sharply varying with wavelength. In that case a further increase in number of terms may not further improve the overall wavelength-normalization curve. To model the U46 ripples present in the W70 + U46

tandem spectrum, 64 Chebyshev terms appear to be sufficient.

Reproducibility of the wavelength normalization can be tested by comparing the λ -curves from data collected on several crystals under the same experimental conditions. The results are illustrated in Fig. 3. The U46 ripples in the W70 + U46 spectrum are reproduced in position and amplitude in all three spectra shown. The two spectra that agree very well (black and green lines) resulted from data collected on crystals of similar size. The third spectrum (red line) is derived from data collected using a somewhat larger crystal. This spectrum deviates from the other two spectra at longer wavelengths. The deviation is attributed to difference in absorption by the crystal and its mount. The spectrum is in a good agreement with the other two spectra when the absorption-correction factor $\exp(A - C\lambda^3 + D\lambda^4)$, appropriate for a spherical crystal (Ren & Moffat, 1995a), is applied.

3.2. Wavelength normalization for U26 data

The wavelength-normalization curve derived for the single-line undulator U26 (17 mm gap) is shown in Fig. 4(a). Data-collection parameters and data-reduction statistics are given in Table 1. The U26 λ -curve is modeled with 64, 128 and 256 Chebyshev terms. Increasing the number of terms from 128 to 256 did not improve the modeling. The error plot in Fig. 4(b) shows no indication of large systematic features at the edges, confirming that modeling with 128 terms is satisfactory. The $(F^2 - \langle F^2 \rangle) / \sigma_{(F^2)}$ residual is flat. It is compressed in the regions of high relative incident intensities while a large random scatter is present as expected in the regions of low intensities. Such observations are rejected prior to merging of the data.

To examine the redundancy of the Laue data needed to derive the U26 λ -curve, we used one frame and five consecutive frames (1° apart) to derive the curve. The one-frame spectrum modeled with 32 Chebyshev terms is shown

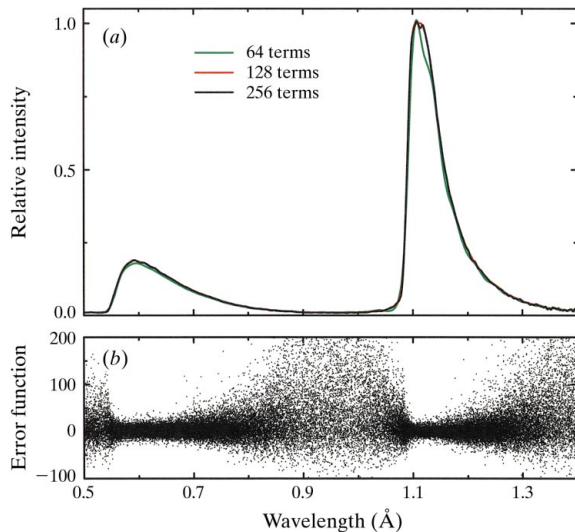


Figure 4 (a) The U26 wavelength-normalization curve derived from PYP data (60 frames, 1° angular increment; one half of the complete data set collected). Differences in the λ -curve as modeled with 64, 128 and 256 Chebyshev terms are shown. (b) The error function $(F^2 - \langle F^2 \rangle) / \sigma_{(F^2)}$ plot for the λ -curve modeled with 256 Chebyshev terms. Large scatter is present in the areas of low intensity but no significant systematic features are present near the edges.

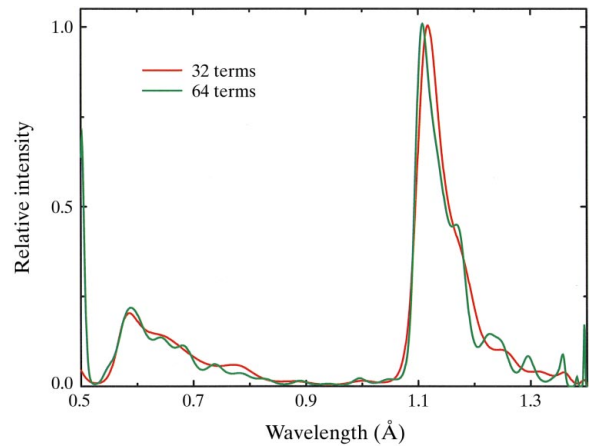


Figure 5 U26 λ -curve derived from one PYP frame with 32 and 64 Chebyshev terms.

in Fig. 5. It already models the fundamental and second-harmonic peaks with roughly the correct shape and intensity ratio of the two peaks although only 282 observations could be used for wavelength normalization in this case. However, such a low number of observations does not permit a further increase in the number of Chebyshev terms to improve modeling of the sharp edges since this introduced artifactual ripples in the spectrum. When five frames are combined (4941 observations), modeling of the λ -curve with 128 terms is possible and is already very satisfactory: the λ -curve agrees well with that derived from

the complete data set (Fig. 4) with only minor small-amplitude artificial ripples. It is therefore not necessary to use an entire data set to derive the wavelength-normalization curve, even in the case of undulator spectra where a high number of Chebyshev terms has to be used to model the sharp rising edges in the spectra. This, of course, is the case only if the absorption by the sample (included in the λ -curve as derived by *LaueView*) is small and does not vary substantially with crystal orientation. Otherwise, the wavelength normalization derived from part of the data may vary from that derived from the entire data.

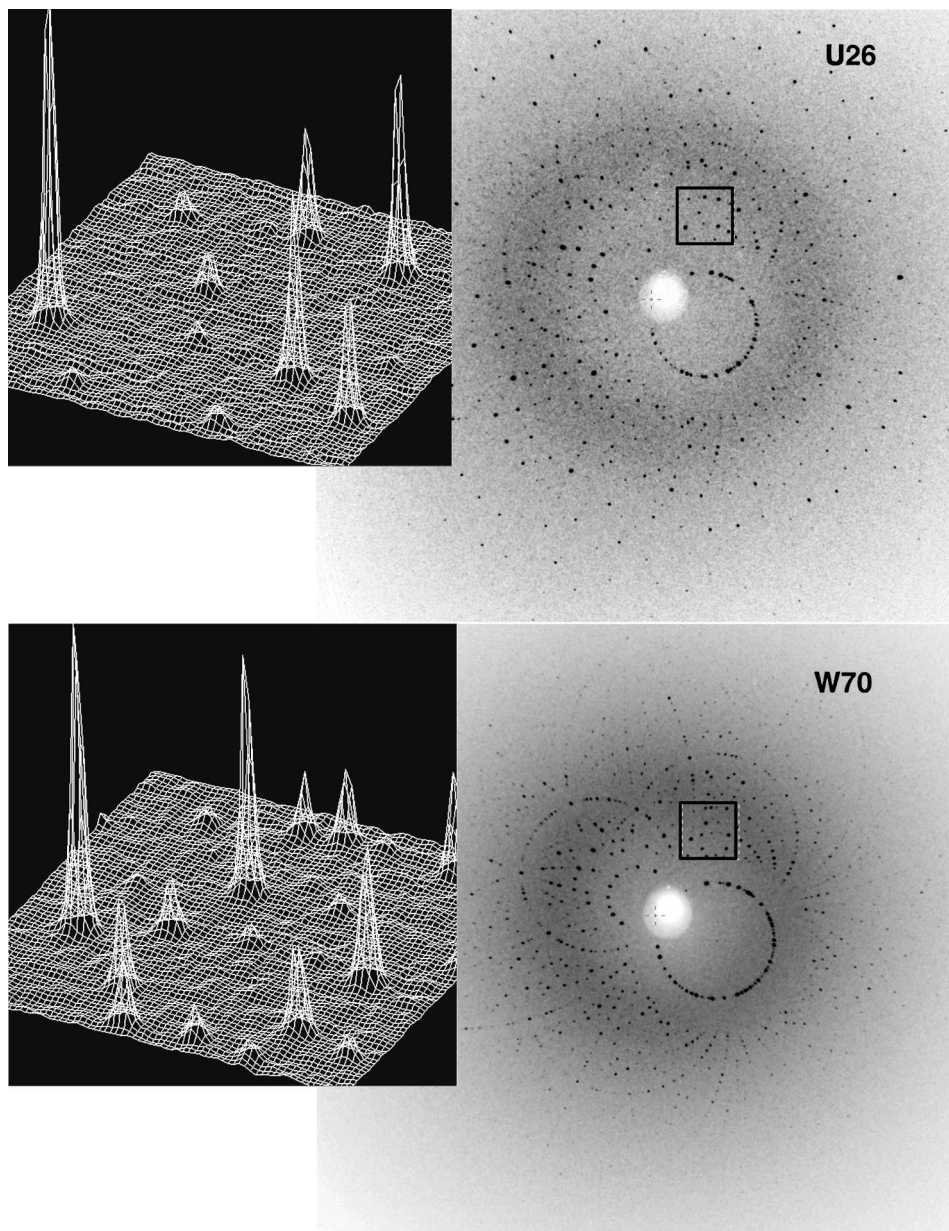


Figure 6

Laue diffraction images for the same PYP crystal collected using U26 and W70 insertion devices. Crystal orientation is not identical but it is very similar. The W70 image is displayed on an intensity scale that is ten times the scale of the U26 image for an easier visual comparison. The surface plots represent the same region of the image (the region is enclosed by the box) in two cases, illustrating the background noise in relation to the diffraction spot intensities. The background level within the dashed box is ~ 40 counts pixel^{-1} for U26 and ~ 580 counts pixel^{-1} for W70. The peak-to-background ratio for the strongest reflection in this box is 34 for U26 and 10 for W70.

The second harmonic of the U26 undulator contributes a very substantial amount of data: about 50% of all measured observations and about 150 unique single reflections, mainly at low resolution. Since the data stimulated by the fundamental peak are quite complete by themselves, the main contribution of the second harmonic is to double the overall redundancy of the data. In the case of single-line undulators, no large contribution of harmonic overlaps is expected due to the narrow bandpass. The presence of the second harmonic in this case, however, significantly improves the data completeness at low resolution by harmonic overlap deconvolution: from 80.1% to 94.0% in the resolution range 100–4.4 Å.

The same PYP crystal used for the U26 data was also used to collect a W70 data set. Data-collection parameters and data-reduction statistics for these data sets are given in Table 1. Two images for an almost identical crystal orientation, one collected with U26 and the other with W70, are shown in Fig. 6. The background recorded at the edge of the detector is 16 times lower for U26: ~ 5 counts pixel^{-1} for U26 and ~ 80 counts pixel^{-1} for W70. The total exposure time per frame was two times longer for W70 so that the true background ratio is about eight. Both W70 and U26 data were collected with the same crystal-to-detector distance (125 mm). This unfortunately limited the resolution of the collected data to 2.2 Å in the case of the quasi-monochromatic U26, with the fundamental at ~ 1.1 Å and a detector size of 140 mm. The second harmonic, with its higher energy but weaker intensity, did not stimulate reflections beyond 2.8 Å resolution. In contrast, the W70 data are quite complete to 1.8 Å.

Similar data-rejection criteria were applied during scaling and before merging of data for both data sets. The value of R_{merge} for both sets is similar: 5.2% for U26 and 4.7% for W70 (Table 1). The overall redundancy is high for both: 13.6 for U26 and 10.1 for W70. This overall comparison is not completely appropriate since the W70 data extend to a resolution of 1.8 Å but the U26 data extend to only 2.2 Å resolution. If data for W70 are restricted to 2.2 Å, the value of R_{merge} is 4.3%. R_{merge} shows some improvement at low integrated intensities and at higher resolution for the U26 data compared with W70. One would expect this trend, as a benefit of the very low background and resulting improvement of the signal-to-noise ratio for each Laue spot. At low resolution and higher integrated intensities, however, R_{merge} is somewhat larger for the U26 data than for the W70 data. In fact, for U26 the value of R_{merge} unexpectedly increases with intensity at the highest intensities. The trend is also evident from the $(F^2 - \langle F^2 \rangle) / \sigma_{(F^2)}$ versus resolution plot shown in Fig. 7 where a scatter in $(F^2 - \langle F^2 \rangle) / \sigma_{(F^2)}$ below 3 Å is much more prominent for U26. This low-resolution behavior is partly due to a large number of reflections in this resolution range that are stimulated by low-intensity wings of the second harmonic (and some by the fundamental). However, this behavior may also arise from difficulties in recording fully integrated intensities at low resolution when

insertion devices with a narrow bandpass, such as U26, are used (Ren *et al.*, 1999). It is estimated (Ren *et al.*, 2000) that only $\sim 30\%$ of reflections at 3 Å are fully recorded with the U26 fundamental for crystals with mosaicity of 0.5° (beam

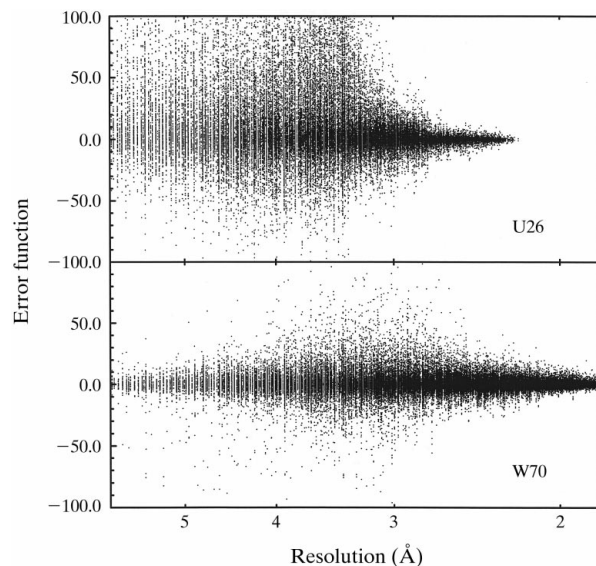


Figure 7

Plot of $(F^2 - \langle F^2 \rangle) / \sigma_{(F^2)}$ versus resolution for U26 and W70. The scatter in $(F^2 - \langle F^2 \rangle) / \sigma_{(F^2)}$ at low resolution is much higher in the case of U26. All the reflections are treated as fully recorded in both cases.

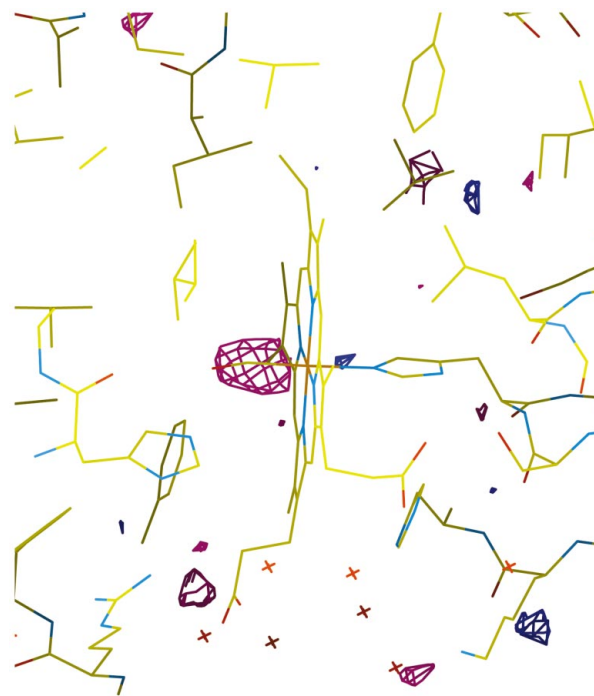


Figure 8

Mb* (3.5 ns) – MbCO difference electron density map at 2.3 Å resolution from U26 data. The map is contoured at $\pm 3\sigma$. Positive density is shown in blue and negative density is shown in red.

divergence is not taken into account). The correlation plot of F/σ_F for the two data sets (not shown) indicates no improvement in the F/σ_F ratio for the U26 data.

Another demonstration of the quality of data collected with U26 is the time-resolved Laue data collected on MbCO crystals. We collected two data sets in the single-bunch mode: one corresponding to MbCO and another corresponding to its photoproduct, Mb*, at 3.5 ns. Photolysis is achieved by illuminating the MbCO crystals by 10 ns laser pulses at 630 nm prior to each X-ray exposure (Šrajer *et al.*, 1996). The wavelength of the U26 fundamental peak and the crystal-to-detector distance again limited the resolution of the data collected to 2.3 Å. The resulting difference electron density map at 2.3 Å resolution is shown in Fig. 8. The loss of the CO ligand due to photolysis is clearly observed (the red feature at the bound-CO location with the peak value of -4.7σ , where σ is the r.m.s. value of the difference electron density in the asymmetric unit). This interpretable difference map from the nanosecond time-resolved Laue experiment testifies to the quality of the single-bunch Laue data collected using the U26 undulator and to the success of the data processing using the *LaueView* software package.

3.3. Wavelength normalization for U20 data

The final insertion device we tested for Laue data collection was the single-line undulator U20 (16.8 mm gap). The wavelength-normalization curve that corresponds to this device (Fig. 9a) was derived from an MbCO data set (Table 2) and is modeled with 128 Chebyshev terms. The corresponding error plot (Fig. 9b) shows a large scatter in the areas of low relative intensity but no significant systematic features warrant a further increase in the number of Chebyshev terms. Owing to the narrow bandpass of the X-ray source, most observations are singles. The harmonic deconvolution therefore only marginally improves the completeness of the data at low resolution in this case, from 93.4% to 94.7% in the 30–4.4 Å resolution range. Similar to the U26 data set, the value of R_{merge} increases rather than decreasing at higher integrated intensities.

The directly measured incident X-ray spectrum for U20 is also shown in Fig. 9(a) for comparison. The spectra are in a good agreement. The differences are attributed to absorption by the crystal and its mount and to other small differences between the exact experimental conditions for the two measurements.

4. Conclusions

Spectral characteristics of synchrotron insertion devices, such as bandpass and spectrum shape, are important for the choice of source for Laue experiments. The choice has been limited in practice by the capabilities of the software for Laue data processing. Owing to the harmonic and spatial overlap problems in data processing, narrower bandpass

sources were originally considered preferable (Moffat *et al.*, 1984; Bartunik & Borchert, 1989; Bartunik *et al.*, 1992). Handling the sharp spectral features in narrow-bandpass spectra was, however, a problem. Very narrow bandpass sources, such as undulators, are attractive since they typically offer higher peak incident intensities and lower polychromatic background in Laue images than broad-bandpass wigglers.

Building on the initial successes of the Chebyshev polynomial method in wavelength normalization with an undulator source (Smith Temple, 1989; Szebenyi *et al.*, 1992), we present here further evidence that this method is powerful and successful in modeling complex wiggler and single-line undulator spectra.

Our limited direct comparison of Laue data collected on the same crystal by both wiggler W70 and undulator U26 did not reveal a clear advantage of one insertion device over the other. The data are very comparable in quality up to 2.2 Å resolution, the limit to which data could have been compared. To answer the broader question of whether wigglers or single-line undulators are better suited for Laue data collection, a more comprehensive comparison is needed. A better comparison would be between the U20 undulator and the W70 wiggler, for example. The second harmonic of the U20 undulator is rejected by the mirror and the polychromatic background is therefore even further suppressed owing to its narrower bandpass. Also, data has to be collected to higher resolution than in our example since the major benefits of improved signal-to-noise ratio are expected for very weak observations at high

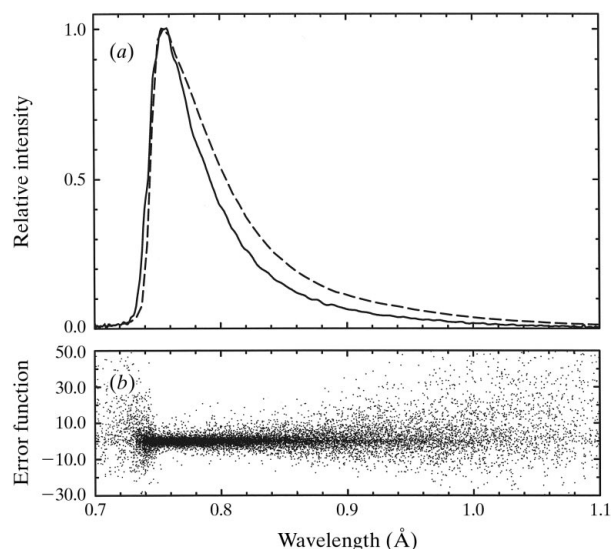


Figure 9
(a) U20 wavelength-normalization curve derived from MbCO data (90 frames, 2° angular increment; half of the complete data set used). The λ -curve is modeled with 128 Chebyshev terms. The measured U20 spectrum is shown for comparison (dashed line). (b) The error function $(F^2 - \langle F^2 \rangle) / \sigma_{(F^2)}$ plot for the λ -curve modeled with 128 Chebyshev terms. No significant systematic features near the edge are present.

resolution. The low-resolution reflections also need to be carefully compared to assess the problem of partials when narrow-bandpass insertion devices are used for Laue measurements. An apparent and important disadvantage of the undulators as compared with wigglers is the large number of frames needed for a complete Laue data set. This becomes important when radiation damage is of concern. It may require several crystals to complete a data set and this will introduce additional errors due to scaling and merging of Laue data from different crystals. In time-resolved Laue experiments where laser pulses are used to initiate structural changes, the crystal is also damaged by a large number of laser pulses. In the case of irreversible systems, each X-ray exposure may require a new crystal. Clearly, in both cases a small number of frames is desirable. Another concern associated with undulator sources is the difficulty in recording full integrated intensities at low resolution when the bandpass of the source is very narrow (Ren *et al.*, 1999). Finally, the increased total elapsed time for the experiment is a serious concern for experiments conducted under severe time constraints at synchrotron facilities.

References

- Arzt, S., Campbell, J. W., Harding, M. M., Hao, Q. & Helliwell, J. R. (1999). *J. Appl. Cryst.* **32**, 554–562.
- Bartunik, H. D., Bartsch, H. H. & Huang, Q. (1992). *Acta Cryst.* **A48**, 180–188.
- Bartunik, H. D. & Borchert, T. (1989). *Acta Cryst.* **A45**, 718–726.
- Bourenkov, G. P., Popov, A. N. & Bartunik, H. D. (1996). *Acta Cryst.* **A52**, 797–811.
- Bourgeois, D., Nurizzo, D., Kahn, R. & Cambillau, C. (1998). *J. Appl. Cryst.* **31**, 22–35.
- Bourgeois, D., Ursby, T., Wulff, M., Pradervand, C., LeGrand, A., Schildkamp, W., Labouré, S., Šrajer, V., Teng, T.-Y., Roth, M. & Moffat, K. (1996). *J. Synchrotron Rad.* **3**, 65–74.
- Campbell, J. W., Habash, J. R., Helliwell, J. R. & Moffat, K. (1986). *Inf. Q. Protein Crystallogr.* **18**, 23–31.
- Campbell, J. W. & Hao, Q. (1993). *Acta Cryst.* **A49**, 889–893.
- Clifton, I. J., Duke, E. M. H., Wakatsuki, S. & Ren, Z. (1997). *Methods Enzymol.* **277**, 448–467.
- Helliwell, J. R., Habash, J., Cruickshank, D. W. J., Harding, M. M., Greenhough, T. J., Campbell, J. W., Clifton, I. J., Elder, M., Machin, P. A., Papiz, M. Z. & Zurek, S. (1989). *J. Appl. Cryst.* **22**, 483–497.
- Moffat, K. (1997). *Methods Enzymol.* **277**, 433–447.
- Moffat, K., Szebenyi, D. & Bilderback, D. (1984). *Science*, **279**, 1423–1425.
- Nieh, Y. P., Raftery, J., Weisgerber, S., Habash, J., Schotte, F., Ursby, T., Wulff, M., Hädener, A., Campbell, J. W., Hao, Q. & Helliwell, J. R. (1999). *J. Synchrotron Rad.* **6**, 995–1006.
- Perman, B., Šrajer, V., Ren, Z., Teng, T.-Y., Pradervand, C., Ursby, T., Bourgeois, D., Schotte, F., Wulff, M., Kort, R., Hellingwerf, K. & Moffat, K. (1998). *Science*, **279**, 1946–1950.
- Ravelli, R. B. G., Raves, M. L., Scheres, S. H. W., Schouten, A. & Kroon, J. (1999). *J. Synchrotron Rad.* **6**, 19–28.
- Ren, Z., Bourgeois, D., Helliwell, J. R., Moffat, K., Šrajer, V. & Stoddard, B. L. (1999). *J. Synchrotron Rad.* **6**, 891–917.
- Ren, Z. & Moffat, K. (1995a). *J. Appl. Cryst.* **28**, 461–481.
- Ren, Z. & Moffat, K. (1995b). *J. Appl. Cryst.* **28**, 482–493.
- Ren, Z. & Moffat, K. (2000). In preparation.
- Smith Temple, B. R. (1989). PhD thesis, Cornell University, USA.
- Šrajer, V., Teng, T.-Y., Ursby, T., Pradervand, C., Ren, Z., Adachi, S., Schildkamp, W., Bourgeois, D., Wulff, M. & Moffat, K. (1996). *Science*, **274**, 1726–1729.
- Szebenyi, D. M. E., Bilderback, D. H., LeGrand, A., Moffat, K., Schildkamp, W., Smith Temple, B. & Teng, T.-Y. (1992). *J. Appl. Cryst.* **25**, 414–423.
- Wulff, M., Schotte, F., Naylor, G., Bourgeois, D., Moffat, K. & Mourou, G. (1997). *Nucl. Instrum. Methods Phys. Res. A*, **398**, 69–84.
- Yang, X.-J., Ren, Z. & Moffat, K. (1998). *Acta Cryst.* **D54**, 367–377.